Solution structure of mannobioses unravelled by means of Raman optical activity

Robert Pendrill,[a] Shaun T. Mutter, [b,c] Carl Mensch,[d,e] Laurence D. Barron,[f] Ewan W. Blanch,[g] Paul L.A. Popelier,[b] Göran Widmalm,[a] and Christian Johannessen*[d]

Abstract: Structural analysis of carbohydrates is a complicated endeavour, due to the complexity and diversity of the samples at hand. Herein, we apply a combined computational and experimental approach, employing molecular dynamics (MD) and density functional theory (DFT) calculations together NMR and Raman optical activity (ROA) measurements, in the structural study of three mannobiose disaccharides, consisting of two mannoses with varying glycosidic linkages. The disaccharide structures make up the scaffold of high mannose glycans and are therefore important targets for structural analysis. Based on the MD population analysis and NMR, the major conformers of each mannobiose were identified and used as input for DFT analysis. By systematically varying the solvent models used to describe water interacting with the molecules and applying overlap integral analysis to the resulting calculational ROA spectra, we found that a full quantum mechanical/molecular mechanical approach is required for an optimal calculation of the ROA parameters. Subsequent normal mode analysis of the predicted vibrational modes was attempted in order to identify possible marker bands for glycosidic linkages. However, the normal mode vibrations of the mannobioses are completely delocalised, presumably due to conformational flexibility in these compounds, rendering the identification of isolated marker bands unfeasible.

Introduction

Carbohydrates constitute a large and very diverse group of biomolecules, ranging from simple sugars to branched polysaccharides and the glycan constituents of glycoproteins. Equally diverse are the functions of this group and their importance is well recognized in protein folding, cell adhesion, immune response and bacterial infections.[1] Yet, compared to proteins, detailed knowledge about the structure of these complex carbohydrates is still lacking. Although analysis by what can be regarded as conventional structure elucidation methods, such as X-ray diffraction and nuclear magnetic resonance (NMR) spectroscopy,[2,3] have resulted in significant understanding of the three-dimensional structure of carbohydrates, further investigations using methodology that can shed light on structural and dynamics details, where the classical methods are limited, are highly valued. With respect to X-ray analysis, it is often difficult to obtain crystals of sufficient quality for natural or unprotected oligosaccharides, even though it is possible in certain cases. However, for larger structures only a limited number has been successfully determined.[4,5] NMR spectroscopy offers a better choice for studies of oligosaccharides in solution, but overlap of spectral resonances quite rapidly become a problem once the size becomes larger. For polysaccharides the repetitive character due to the repeating units makes spectral interpretation essentially impossible based on an atom-by-atom basis. As a result, any analysis needs to be performed with respect to averaged structures along the polymer chain.[6] However, by combining results from NMR with extensive MD simulations, a good deal of information can be obtained. Molecular structures can be interpreted and established as populations of conformations with identification of the low potential energy conformations as important representatives of the carbohydrate structure,[7,8] which may also be important for investigating interactions with proteins.[9,10] Hence, there is a need to broaden the toolbox available when performing structure elucidation of carbohydrates, in order to assist the current techniques.

The optical spectroscopic technique Raman optical activity (ROA) has previously shown great promise as a complementary method in the structural analysis of carbohydrates.[11-22] ROA is based on classical Raman scattering, where inelastic light scattering (usually from a laser source) results in a difference in energy from of the Raman scattered photons with respect to the incident photon energy. In Raman spectroscopy, plotting these shifts in wavenumbers (cm^{-1}) *versus* scattering intensity results in a spectrum similar to an infrared absorption spectrum, as Raman is probing the vibrational frequency range. ROA further sensitizes Raman spectroscopy by introducing sensitivity to asymmetry and

[a] Dr. R. Pendrill, Prof. dr. G. Widmalm
Department of Organic Chemistry, Arrhenius Laboratory
Stockholm University
S-106 91 Stockholm, Sweden.
[b] Dr. S.T. Mutter, Prof. dr. P.L.A. Popelier
Manchester Institute of Biotechnology
University of Manchester
131 Princess Street, Manchester M1 7DN, UK.
[c] Dr. S.T. Mutter
Department of Natural Sciences
Middlesex University
NW4 4BT London, UK.
[d] Dr. C. Mensch, Prof. dr. C. Johannessen*
Department of Chemistry
University of Antwerp
Groenenborgerlaan 171, 2020, Antwerp, Belgium.
Email: christian.johannessen@uantwerpen.be
[e] Dr. C. Mensch
Ghent Quantum Chemistry Group
Department of Chemistry
University of Ghent
Krijgslaan 281, 9000 Ghent, Belgium.
[f] Prof. dr. L.D. Barron
School of Chemistry
University of Glasgow
Joseph Black Building, Glasgow G12 8QQ, UK.
[g] Prof. dr. E.W. Blanch
School of Science,
RMIT University
GPO Box 2476, Melbourne, VIC, 3001, Australia.

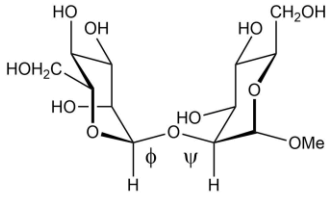

M2M

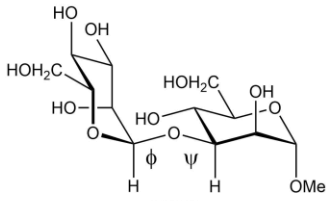

M3M

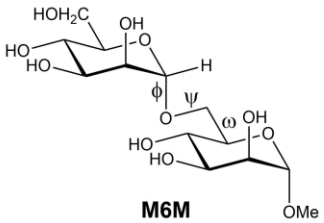

M6M

chirality, achieved by measuring a small difference in Raman scattering of right- and left-circularly polarized light, scattered by chiral molecules.[23-25] The resulting difference spectrum is usually better resolved than the parent Raman spectrum, and sensitive to chirality (e.g. enantiomers display mirror image ROA). The technique is extraordinarily sensitive to the immediate environment around chiral centers, and has been used extensively to study biomolecules in aqueous solution, from single amino acids and monosaccharides, to peptides, proteins, glycoproteins and even intact viruses.[26-28] This sensitivity has been shown experimentally to be transferable to carbohydrates,[11-22] due to the highly chiral nature of these compounds.

As for all optical spectroscopic techniques, the main challenge for ROA lies in interpreting the spectral data obtained from experiment. Here, spectroscopists nowadays turn to quantum mechanical calculations, specifically density functional theory (DFT), modelling low energy conformations of the target molecule, and calculating predicted spectral data for comparison with experiment and normal mode analysis.[28-32] Several such combined experimental and theoretical studies of carbohydrates using ROA as the experimental tool have previously been carried out.[17,19-22] Among these, protocols have been developed for the detailed study of monosaccharides, using MD population analyses to generate a number of representative structural conformations with explicit solvation.[19-22] These structures are then further geometry optimized, in order to prepare them for ROA property tensor calculations. This procedure has been performed at a number of levels of theory, ranging from gas phase calculations to the quantum mechanical/molecular mechanical (QM/MM) level, in order to understand the relationships between monosaccharide stereochemistry, functional group interactions and orientation, and the role of solvation interactions in regulating the conformational dynamics of small sugars.[19-22]

In this study, we expand our systematic combined ROA/modeling study of carbohydrates to include disaccharides, viz., the three mannobioses α-D-Man*p*-(1→2)-α-D-Man*p*-OMe (**M2M**), α-D-Man*p*-(1→3)-α-D-Man*p*-OMe (**M3M**) and α-D-Man*p*-(1→6)-α-D-Man*p*-OMe (**M6M**) (Figure 1).

These three disaccharide structures are the main components of high-mannose glycans, constituting not only the mannose unit itself but also three different glycosidic linkages.[33] Due to their importance as signatures in high-mannose glycoproteins, these three mannobioses have previously been studied using NMR spectroscopy, MD simulations and X-ray crystallography.[34-38] Furthermore, experimental ROA studies of these three compounds have been reported.[39] The study by Johannessen *et al.* showed that while the parent Raman spectral profiles of the three mannobioses is very similar, this is not the case for the ROA spectra, indicating a sensitivity towards the difference in glycosidic linkage.[39] While ROA signatures have been proposed for different glycosidic linkages from experimental studies,[12,13] there has been no previous reported ROA or Raman investigation into how different glycosidic linkages affect the interactions between monosaccharide moieties or how this then differentiates structural motifs in oligosaccharides and glycans.

Here, we carry out a qualitative and quantitative (overlap integral analysis) evaluation of DFT level calculations of the three mannobioses at gas phase, dielectric continuum (CPM), solvent restricted and non-restricted QM/MM and explicit solvation (QM

Figure 1. The structures of **M2M**, **M3M** and **M6M**.

water; Also including a CPM background) levels. Our results show that the combined computational approach developed for monosaccharides can be applied to larger carbohydrates, further expanding the role of ROA in structural biology.

Results and Discussion

Population analysis

Based on the MD production runs, the main conformations of all three mannobioses could be identified. For **M2M**, the ψ torsion angle populated two states with positive and negative values to 58% and 42%, respectively. This population distribution correctly identifies the major and the minor states and can be compared to the ~3:1 distribution found by NMR and optical rotation data in conjunction with an X-ray database search of structural elements containing the disaccharide.[40] From the herein performed MD simulation the averages of the ψ torsion angle in the two states were 38° and −13°, respectively.

In **M3M**, the ψ torsion angle populated two states with average torsion angles of 53° and −8°, respectively, in a 17% to 83%

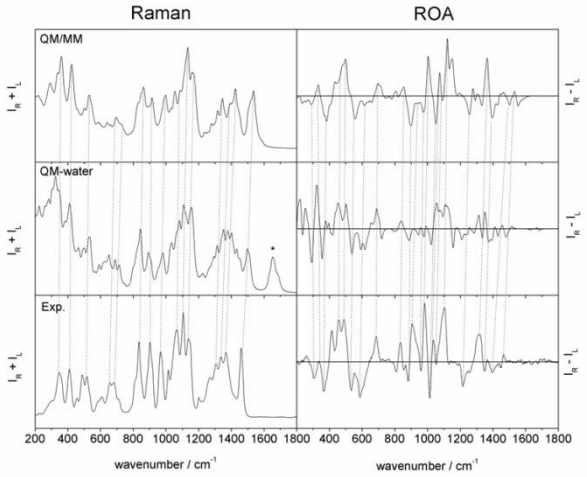

ratio. From NMR spectroscopic data, the $^{3}J_{C1',H3}$ coupling constant in **M3M** was determined to be 5.0 Hz and the $^{3}J_{H1',C3}$ coupling constant was found to be 3.8 Hz. The corresponding values calculated from the MD trajectory were 5.2 and 3.8 Hz, respectively, using the JCX/SU09 Karplus equations,[40] which is within the experimental error of the NMR measurement. Analysis of the MD simulation showed that the $^{3}J_{C1',H3}$ coupling constants were 2.5 and 5.7 Hz for the positive and negative conformers of the ψ torsion angle, respectively. The experimental value corresponds to a 1:4 ratio of these two states. Hence, a final weighting of **M3M** was set to a 20% to 80% ratio as an average of these two ratios.

The α-(1→6)-linked disaccharide **M6M** showed flexibility at both the ψ and ω torsion angles whereas for the ϕ torsion angle the *exo*-anomeric conformation prevailed, leading to the identification of five different conformations from the MD simulation. The *antiperiplanar* (*ap*) conformation of ψ returns values close to 180° with a population of 87% during the trajectory, with the remainder being in a *clinal* (+*cl*) conformation having values close to +90°, similar to what was observed in a previous MD simulation of **M6M**.[41] The ω torsion angle populated the *gt* (ω ≈ +60°), *gg* (−60°), and *tg* (180°) rotamers in a 0.32:0.68:0.00 ratio over the whole trajectory. The ratios of these conformations were found to correlate with the conformation at the ψ torsion angle, with the *ap*-conformation having a 0.23:0.77:0.00 ratio while the +*cl*-conformation showed a predominant population of the *gt* conformation, resulting in a 0.92:0.08:0.00 ratio. Experimental NMR data on **M6M** have resulted in the relative populations for the ω conformational states as 45:49:6 for *gt*:*gg*:*tg*, respectively.[42] Hence, based on the experimentally determined ω conformational distribution and the fact that a small amount of the +*cl* conformation at the ψ

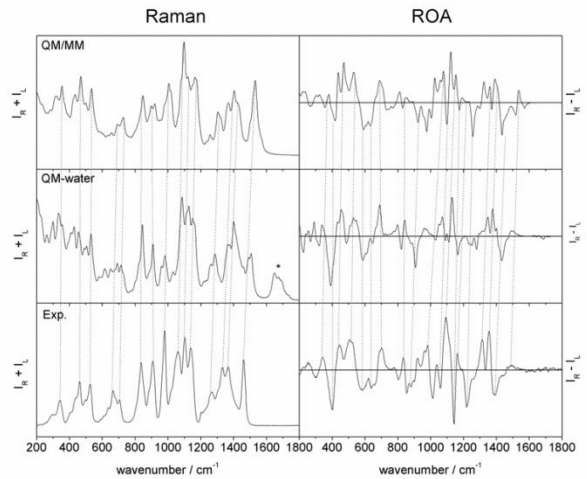

torsion angle was observed in the MD simulation the five states and relative populations selected for the subsequent analysis were *gt*:*ap* (40%), *gt*:+*cl* (5%), *gg*:*ap* (44%), *gg*:+*cl* (5%), and *tg*:*ap* (6%).

Raman and Raman optical activity: Qualitative comparison

In previous experimental studies of carbohydrate ROA spectra, empirical analyses have led to assigning certain regions of the ROA spectra to different types of normal mode vibrations.[12] These regions are referred to as the low wavenumber/anomeric region (below ~950 cm^{-1}), the fingerprint region (~950-1200 cm^{-1}) and the deformation region (~1200-1500 cm^{-1}). The low wavenumber region, while being dominated by delocalized modes, has empirically been assigned to signatures sensitive to linkage
type and anomeric configuration. The fingerprint region has shown some sensitivity to linkage type and the shape of the deformation region has been associated with CH_2OH rotamer distribution.[12] While this spectral nomenclature is still readily used, including this paper, recent DFT studies of

Figure 2. Raman (left) and ROA (right) of the full QM/MM calculations (upper) and explicit QM water calculations (middle) compared to experiment (lower) of **M2M**. Major spectral bands used in the qualitative comparison are marked by dotted lines. The * marks vibrational water modes in the QM water calculation.

Figure 3. Raman (left) and ROA (right) of the full QM/MM calculations (upper) and explicit QM water calculations (middle) compared to experiment (lower) of **M3M**. Major spectral bands used in the qualitative comparison are marked by dotted lines. The * marks vibrational water modes in the QM water calculation.

monosaccharides indicate a more complicated nature of the normal mode distribution in carbohydrates.[20,21]

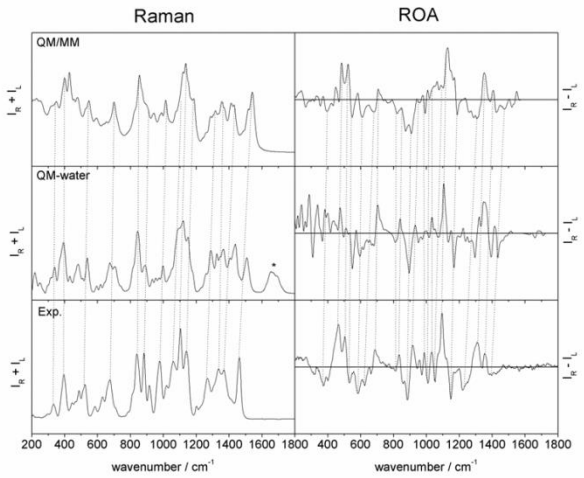

Figure 4. Raman (left) and ROA (right) of the full QM/MM calculations (upper) and explicit QM water calculations (middle) compared to experiment (lower) of **M6M**. Major spectral bands used in the qualitative comparison are marked by dotted lines. The * marks vibrational water modes in the QM water calculation.

From the population analysis carried out above, representative MD snapshots of all main conformations of the mannobioses were chosen for DFT level calculations and subsequent comparison with experiment. The experimental data was previously reported by Johannessen et al.[39] and in Figures 2, 3 and 4, experimental Raman and ROA data of **M2M**, **M3M** and **M6M**, respectively, are compared to predicted data from the QM/MM and QM water levels of theory. For sake of completeness, the equivalent predicted data, calculated in gas phase, CPM and restricted solvent QM/MM, are presented in the Supporting Information (SI), in Figures S1, S2 and S3.

For the three mannobioses, experimental Raman and ROA
spectra were collected, with significant spectral data all the way from the low wavenumber region to the deformation region.[39] While the experimental Raman spectra are very similar, initially indicating that the main normal mode contribution to the Raman spectra originates from each mannose unit per se, the three experimental ROA spectra are clearly different. This finding verifies that ROA spectra are more sensitive than Raman spectra to oligosaccharide conformation. Even so, there are also overlapping trends in each of the diagnostic regions, making a purely experimental assignment of marker bands to specific linkage type and conformation impossible.

Comparing the experimental and predicted data, a more complicated picture emerges. In general, with a couple of exceptions, the predicted spectra calculated at the QM/MM or QM water level compare decently with experiment, which results from the complicated computational schemes implemented and is also a testimony to the validity of the population analysis. Thus, in order to attempt making a band assignment, it is very useful to identify the best computational approach (here, assuming that the lower level methods presented in the SI are of inferior quality) and only use this data when performing the band assignment.

In the case of **M2M**, qualitative inspection of the spectra in Figure 2 favours the QM/MM calculation over the explicit QM water calculation, in particular when comparing ROA data. With the exception of a few bands, most experimental ROA bands can be directly assigned to an equivalent predicted band for all three regions defined above. This is not the case for the QM water calculation, in particular with respect to the fingerprint region where overlap with the experimental spectrum is considerably less pronounced.

Intriguingly, the superiority of the QM/MM approach observed for **M2M** is not repeated for **M3M**. In this case, comparison between experiment and predicted data is much less straightforward, as qualitative studies favour QM water in some regions of the ROA spectra and QM/MM in others. Additionally, the fingerprint region is not particularly well predicted by either of the two computational approaches. On a very loose basis, the QM water-based calculations could be the preferred ones when the ROA data is considered, but this is not a clear-cut decision. This ambiguous trend follows in the Raman spectra, where it is difficult to determine if one method provides better comparison than the other.

For **M6M**, the qualitative comparison becomes even more difficult. Comparing the ROA data, the low wavenumber region clearly favours the QM/MM calculation as the two strong positive bands that are surrounded by broad negative features are quite well reproduced in the QM/MM spectrum and not at all in the QM water spectrum. On the other hand, the fingerprint region clearly favours the QM water calculation with a close to perfect overlap of bands. Finally, the deformation region, from 1200-1500 cm^{-1}, shows a very good overlap between the QM/MM calculated spectrum and experiment, beating the performance of the QM water calculations in this region. Unfortunately, both calculated Raman spectra compare relatively poorly (compared to **M2M** and **M3M**) to the experimental spectrum and offer little help in choosing the right computational approach.

In summary, as this simple visual and qualitative analysis of the predicted data does not lead to an evident conclusion, a more quantitative (and less subjective) analysis is warranted.

Overlap integral analysis

Traditionally, assignment of ROA data has been based on the simple qualitative band assignment by visually overlapping data, as attempted in the previous section. In this case, and in other cases with complex spectral data, an added level of confidence in band assignment can be gained by quantitatively determining the level of overlap,

Table 1 Similarity S_{fg} (%) calculated for the ROA and Raman spectra, based on the optimal scaling factor (SF) for the ROA spectra. The highest S_{fg} value is marked out for each compound.

	Method	M2M		M3M		M6M	
		S_{fg}	SF	S_{fg}	SF	S_{fg}	SF
ROA	Full QM/MM	69.6	0.970	57.3	0.969	72.1	0.967
	Restricted QM/MM	48.2	0.984	54.9	0.977	55.0	0.980
	QM water	48.0	0.991	62.6	0.978	59.0	0.986
	CPM	48.1	0.993	68.3	0.983	57.9	0.998
	Gas	45.4	0.993	31.2	0.972	58.4	0.993
Raman	Full QM/MM	89.4	0.970	88.8	0.969	87.2	0.967
	Restricted QM/MM	82.7	0.984	86.1	0.977	84.0	0.980
	QM water	76.0	0.991	85.1	0.978	90.6	0.986
	CPM	85.5	0.993	84.6	0.983	87.2	0.998

	Gas	78.7	0.993	77.9	0.972	80.6	0.993

e.g. integral analysis.[43-48] The method applied here calculates the normalized integral overlap, returning a percentage overlap (S_{fg}), ranging from 100% for identical spectra to -100% for mirror image spectra (in the case of ROA; 100% to 0% for Raman). Taking all the predicted data available, where each spectrum has been calculated at the given level and the final weighted average is based on the population analysis; the S_{fg} values were calculated for all three mannobioses, and can be found in Table 1.

Table 1 reveals some very interesting trends. As already determined in the qualitative comparison, **M2M** has a clear computational preference, and assigns a much higher overlap between experiment and the full QM/MM calculation than any of the other methods. Quite unexpectedly, the other S_{fg} values, from the computationally very expensive QM water approach and down to the simple gas phase calculation, are numerically very similar. If the S_{fg} values are to be objectively viewed as a descriptor of quality for a certain calculation, one would expect a clear number hierarchy to emerge, favouring the computationally intensive and time-consuming calculations. Hence, with the current S_{fg} values, it would be very difficult to choose a favoured approach from these numbers alone, as they could, incorrectly, indicate that a lower level calculation may in fact be favourable.

The overlap integral analysis of **M3M**, compared to that of **M2M**, is conspicuous: in the case of the ROA spectra, the highest overlap appears to be between experiment and the CPM dielectric continuum model. The S_{fg} value for the full QM/MM calculation is significantly lower than for CPM. This is in contrast to the Raman spectra, where the overlap integral analysis favours the full QM/MM calculation. Visual inspection of the predicted CPM data presented in Figure S2 supports this analysis fully: the predicted CPM ROA spectrum has very clear similarities with the experimental spectrum. On the other hand, the gas phase calculation for **M3M** is in this case clearly the inferior method.

Equal to the visual overlap analysis of **M6M**, the overlap integral analysis of this compound is somewhat ambiguous: while the full QM/MM calculation has the highest S_{fg} value in the case of the ROA spectra, the QM water calculation is favoured for the Raman spectra. As for **M2M**, the ROA S_{fg} value for the full QM/MM calculation of **M6M** is significantly higher than those of the other methods. Moreover, none of the ROA S_{fg} values for **M6M** are very low, indicating that they all provide reasonable predictions of the experimental spectrum, and the gas phase calculation is, in this case, competing with QM water for the second highest value, while clearly being the lowest value in the case of the Raman spectra.

These results were not anticipated and led us to more closely examine the ROA S_{fg} values of **M2M** and **M3M** as a function of conformational weighting, varying the weights of the two conformations from zero to one hundred percent and calculating the S_{fg} in one percent integrals. **M6M** was not included in this analysis due to the more complicated conformational space, described herein by five conformations. This weight investigation can further be justified by viewing the variational analysis of the two other mannobioses having only two degrees of freedom at the glycosidic linkage as a test of the robustness of the computational approaches in general; e.g. does the largest S_{fg} value coincide with the weight predicted by the population analysis?

The results of this analysis are presented in the SI in Figures S4-S13 and reveal several trends. In the case of **M2M**, the most important finding is that varying the weights for the full QM/MM calculation reveals that the ROA calculations are very robust in this case, e.g. both conformations have high S_{fg} values on their own. Additionally, the highest S_{fg} is found at the ratio 0.59:0.41, which is almost identical to the ratio found in the population analysis, clearly demonstrating that the MD simulation not only finds the correct conformations but also the correct ratio. In contrast, the QM water calculations overshoot the ratio by finding the highest S_{fg} value at 0.80:0.20 while the restricted QM/MM calculation not only finds the highest S_{fg} value at 0.19:0.81 but the overlap of the positive conformation on its own is less than 20%, which indicates that the reoptimisation of the structure has resulted in an incorrect conformation. Curiously, while in general returning lower S_{fg} values than the QM/MM calculation, the gas phase calculations of **M2M** also finds the correct ratio (0.57:0.43) of conformations and appears to be robust for both conformations.

The observations made above are very important when analyzing the overlap integrals calculated for **M3M**. With these, it is clear that the surprisingly good overlap between experiment and CPM calculations is somewhat of a coincidence. While the ROA spectrum of the negative torsion angle conformation has a high level of similarity with experimental data, the ROA spectrum of the positive torsion angle conformation does not compare well with experiment. The analysis finds the highest S_{fg} value at the ratio of 0.13:0.87, close to the ratio of 0.20:0.80 used to generate the weighted spectra. But, the S_{fg} values then drop significantly, from close to 70% towards 25% when adding a significant spectral contribution from the positive torsion angle conformation. Even though this conformation is the minor contribution to the average ROA spectrum of **M3M**, this response clearly indicates that the reoptimisation has significantly altered the structure of this conformation, making the data less reliable and the good overlap for the negative torsion angle conformation probably coincidental.

Interestingly, the full QM/MM calculation for **M3M** finds the highest S_{fg} value not at 0.20:0.80 but at 0.51:0.49, calling for a much higher spectral contribution from the positive torsion angle conformation. Both the restricted QM/MM and QM water calculations find maximum values closer to the ratio taken from the population analysis, although the QM water data seem to be less robust than the full QM/MM data. Finally, as was observed for **M2M**, the gas phase calculations for **M3M** have lower S_{fg} values but agree (almost) with the full QM/MM calculation with respect to the conformer ratios. In order to determine whether this new ratio of conformations has a positive effect on the spectral data, predicted Raman and ROA data of **M3M** at the full QM/MM and QM water levels are compared to experiment in Figure 5, using the ratio 0.51:0.49 to weight the conformations.

Compared to Figure 3, the better overlap between full QM/MM and experiment appears to originate mainly from the low wavenumber region and to some extent the deformation region. Unfortunately, the fingerprint region does not gain much in quality when changing the weights because the strong negative ROA band above 1100 cm^{-1} is still missing from the predicted data and the strong positive band from this resulting couplet (right below 1100 cm^{-1}) appears to split in both the full QM/MM and QM water calculations.

In order to further study how much each region of the computed spectra contributes to the total S_{fg} values, the partial values for the low wavenumber, finger print and deformation regions were calculated for all three mannobioses at all levels of theory, see Figure 6.

From Figure 6, a number of observations can be made concerning the impact of the different regions on the overall similarity indices versus the level of computational complexity. For all three mannobioses, the addition of explicit solvent molecules appears to distribute the similarity with experiment more evenly over the different regions, indicating a general better fit between experiment and theory. For both **M2M** and **M6M**, the finger print region compares better with experiment when using the full QM/MM approach, while for **M3M**, the deformation region is best described by this computational method. In fact, for four out of the six sets of S_{fg} data, the full QM/MM approach

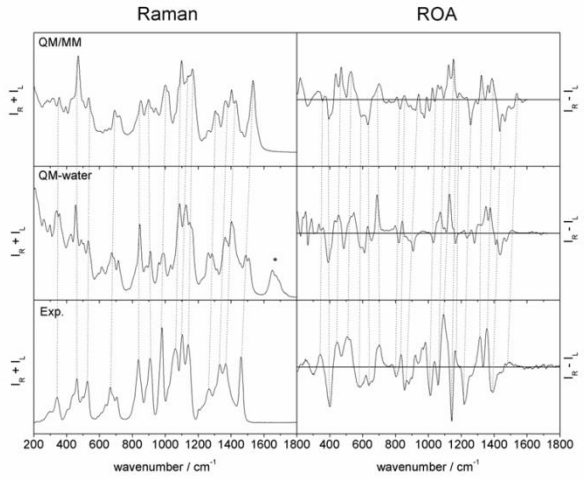

Figure 5. Raman (left) and ROA (right) of the full QM/MM calculations (upper) and explicit QM water calculations (middle) compared to experiment (lower) of **M3M** using the 0.51:0.49 ratio to weight the predicted spectra. Major spectral bands used in the qualitative comparison are marked by dotted lines. The * marks vibrational water modes in the QM water calculation.

gives the best overlap, while the restricted QM/MM approach is outperformed by the CPM dielectric background. The most computationally expensive approach, QM water, does not give the best overlap in any region. This is likely due to this methodology requiring averaging of different explicit solvation configurations, sampling different positioning of water molecules on each sugar conformation, which would render the method prohibitively computationally demanding. Another factor that can influence the overall similarity between experiment and the QM water level predicted spectra, particularly the Raman spectra, is the included calculation of water modes. In the experimental Raman spectra, the solvent bands are subtracted, but as the normal modes of the samples are very delocalised (see the following section), removing normal mode contributions of water from the predicted spectra is not possible. Hence, the QM water predicted spectra includes contributions from water in the spectra, most visible in the Raman spectra above 1600 cm^{-1} (not included in the overlap integral analysis), while the experimental spectra does not. On the other hand, the QM/MM calculations do not include explicit water modes, as the lower level of theory excludes the solvent molecules from the Hessian matrix. Furthermore, in the full QM/MM approach, the sugar conformations are embedded in a responsive molecular mechanics force field, which should lead to a better sampling of the potential energy surface, thus resulting in an overall better fit with experiment.

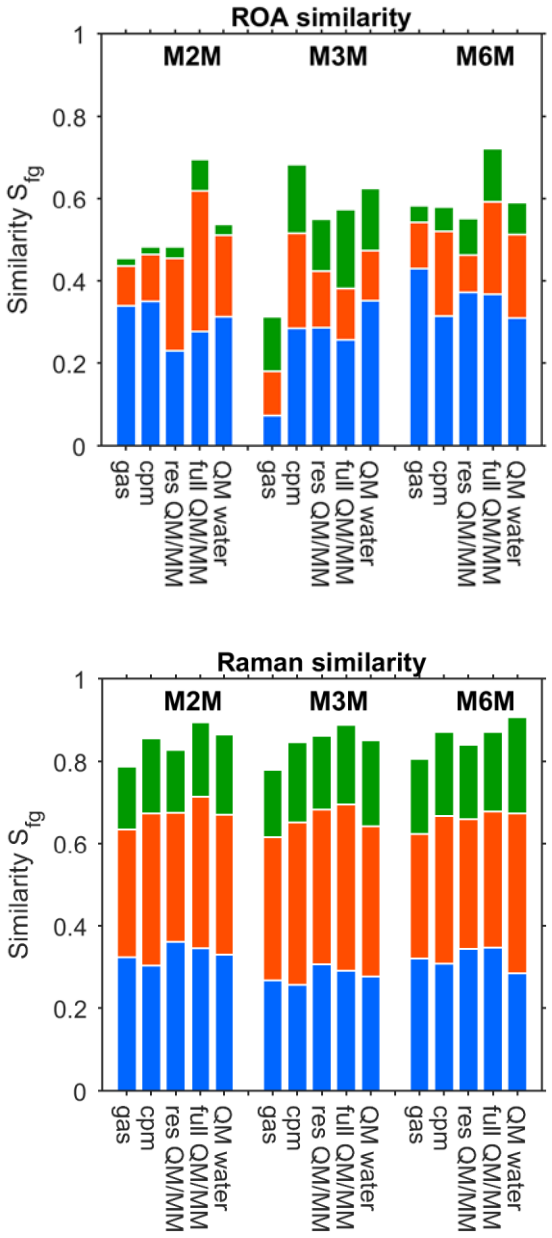

Figure 6. ROA (top) and Raman (bottom) similarities S_{fg} for the different spectral regions: Blue: 300 - 950 cm-1; Orange: 950 – 1200 cm-1 ; Green: 1200 – 1500 cm-1 and for the different computational approaches (1) "gas"; (2) "cpm"; (3) "res(tricted) QM/MM"; (4) "full QM/MM"; (5) "QM water".

Normal mode analysis

Based on the analysis above, the full QM/MM level calculations were chosen as the basis for an attempt at assigning normal mode vibrations to the prominent ROA spectral features in each of the three mannobioses. Previous computational studies of monosaccharides[20,21] have shown that unambiguous assignment of isolated normal modes is difficult in carbohydrates because the rings and the repeating bond type has a tendency to delocalize the normal modes, i.e. everything moves at the same time. We had hoped that for the three mannobioses, marker bands for linkage type could be identified as part of the normal mode analysis, but due to the highly delocalized nature of the normal modes of these molecules, such an assignment is not straight forward.

In the low wavenumber region, all observed bands can be assigned to fully delocalized breathing modes. Due to the fully delocalized nature of these modes, it is not possible to differentiate them or to identify any trends that are molecule-specific except for one: in **M6M**, the CH_2 group being part of the (1→6)-linkage has larger displacement vectors in some normal modes than in others but this does not lead to any specific band structure in the ROA spectrum and hence not any identifiable

marker bands. While this computational assignment does verify the previous empirical assignment to delocalized modes, there is no indication from the current results that the region is sensitive to linkage type in the case of the mannobioses.
In the fingerprint region, traditionally assigned to linkage-type sensitive normal modes due to the prevalence of C-C and C-O-C stretching vibrations in this range, the picture from the previous paragraph repeats itself. While being dominated by C-C stretching modes in the hexose rings and C-O-C stretching modes over the glycosidic bond, there does not appear to be any correlation between linkage type and band profile. This is again most likely to be due, in part, to the delocalized nature of the normal modes: no isolated C-O-C or CH_2-O-C vibrations could be identified, and the combination of C-C ring modes and glycosidic bond stretching modes removes all unique band profile from the different mannobioses.
Finally, in the deformation region, it is not even anticipated to find linkage-sensitive modes, as this region is dominated by C-H and CH_2OH deformation vibrations. Again, the calculations verify the empirical assignment, as this is indeed the case. In fact, C-H and O-H deformation modes from the hexose rings dominate the region in all three cases, with minor contributions from CH_2OH deformations in the cases of **M2M** and **M3M**, again not leading to any conformation-specific bands. In **M6M**, contributions from CH_2OH could not be identified, but this is most likely due to the simple band profile of this region, with only four ROA bands available.
While marker bands cannot be immediately identified, there is, however, an additional factor to consider. While correlation of ROA bands to distinct vibrational modes for sugars in cyclic form can be challenging to establish, as mentioned above, we have been successful in previous studies on several monosaccharides.[19-22] This is the first report of this strategy being systematically applied to disaccharides and the lack of a similar systematic performance of the different solvation modeling approaches is, at first, surprising. We surmise that this difference in the performance of modeling solvent effects on conformational dynamics for disaccharides compared to monosaccharides is due to the complex competition between intramolecular (i.e. between the neighbouring saccharide subunits) and solvent water (i.e. between a saccharide subunit and local water molecules) hydrogen bonding. While the water molecules in the QM/MM model are only represented by point charges, Liem and Popelier have shown that this description is still reasonable in the case of hydrogen bonding (except for small clusters).[49] Naidoo and Chen investigated how the competition between intramolecular and water-carbohydrate intermolecular hydrogen bonds affected the torsional flexibility of the glycosidic linkages in maltose and α-D-GlcNAc-(1⟶4)-β-D-Glc3NH_2).[50] Their MD/*ab initio* study showed that these two types of hydrogen bonds are of similar strength and compete fairly equally with each other, interchanging regularly within the first hydration shell. This may then have a significant effect on the conformational fluctuations at the glycosidic linkage. Furthermore, Wang et al. established that this is particularly important for solvent-exposed intramolecular hydrogen bonds, leading to a conformational steering force.[51] Wang *et al.* also suggested that this leads to the conformational preferences of oligosaccharides being largely driven by steric and stereoelectronic effects.
It is, therefore, likely that the difference in stereochemistry of the three glycosidic linkages investigated in this study will have diverse effects on the competition between intramolecular and solvent water hydrogen bonding partners for each functional group near the glycosidic linkage. The variable levels of performance of our different solvation models, in particular QM/MM vs QM water, is then a consequence of differences in the balance between competing inter- and intra-molecular hydrogen bonding patterns exhibited by the three mannose disaccharides. This is especially important when considering how the different computational models treat the roles of saccharide-water intermolecular hydrogen bonding in the vicinity of the glycosidic bond. While we do not yet have a detailed understanding of the resulting ROA band patterns, probably due to current limitations in how accurately solvation models account for these complex and interchanging hydrogen bonding patterns, this work shows that we are detecting the subtle effects of solvent interactions on disaccharide conformation.
The lack of informative marker bands in the mannobioses is intriguing, as this indicates a lack of spectral sensitivity in ROA towards conformational differences in carbohydrates. This is in contrast to the main body of previous empirical and computational carbohydrate ROA, where many spectral trends have been identified, indicating sensitivity to linkage type and even higher order structure.[12,13,16,18,39,52] Thus, the mannobioses appear to be a special case. Examining the main conformers of the three mannobioses (**M2M** positive, **M3M** negative and **M6M** *gg-ap*), in all three cases, the chair conformation of the two mannose units are very similar, the CH_2OH rotamer population is essentially the same in **M2M** and **M3M** (with **M6M** obviously not comparable here) and even considering that the anomeric configuration at the *O*-methyl group has the same orientation to the hexose ring in all three structures. Thus, the only difference is the linkage type and this study indicates that ROA is less sensitive to this structural difference in this particular case. That said, while the results presented here do not identify any linkage-type specific marker bands, the band profile as a whole can distinguish between the three mannobioses, and clearly verifies the quality of the MD population analysis.

Conclusions

In this paper, we present a detailed conformational study of disaccharides in solution, combining MD simulations, DFT calculations and experimental Raman and ROA spectroscopy to study the vibrational modes of three mannobioses. Due to the complexity of the spectral patterns of these samples, overlap integral analysis comparing the experimental data with the predicted spectra generated at different levels of theory was employed in an attempt to quantify the spectral quality of the calculations.
From these results, we show that the vibrational modes of the investigated mannose disaccharides are highly delocalized, much more so than for previously investigated monosaccharides,[17,19-22] and that marker bands could not be identified for the glycosidic linkages within these three disaccharides. This is in contrast with a study performed on agarose polysaccharides,[52] where a similar combined

computational and experimental ROA approach revealed a systematic sensitivity towards higher order structure. Previous studies of other disaccharides by ROA spectroscopy also seem to show clear glycosidic signatures as inferred in the discussion and that mannose therefore may be a special case. The rather nebulous ROA results, and especially the absence of any clear marker bands for the glycosidic linkage, might be construed as indicative of conformational freedom around the glycosidic linkages, which tends to average out the ROA signals. Due to the short timescale of Raman scattering (compared to NMR), ROA provides a direct snapshot of all the separate interconverting conformers present in the sample, while NMR provides a global time average. Our results appear to reveal that mannose oligomers do indeed exhibit unusual and remarkable flexibility compared with other carbohydrates that have been studied, on account of the high level of delocalisation of the vibrational normal modes. This is not in conflict with the MD population analysis, as the normal mode delocalisation indicates conformational freedom on a short time scale, suggesting local flexibility rather than a whole-scale change in conformation. Thus, this remarkable and unusual conformational freedom may have functional significance for mannose oligomers as the key constituents in the glycan chains of glycoproteins.

Experimental Section

NMR spectroscopy.

Experiments were performed with **M3M** obtained from Carbohydrates International AB (Arlöv, Sweden) in D_2O at 303 K on a Bruker Avance III 700 MHz spectrometer equipped with a 5 mm TCI Z-gradient cryoprobe.

Heteronuclear long-range $^{13}C,^{1}H$ coupling constants were determined using the J-HMBC experiment.[53] One-bond $^{13}C,^{1}H$ correlations were suppressed by a low-pass J filter having τ_1 = 3.45, τ_2 = 3.13 and τ_3 = 2.78 ms. Hard ^{13}C 180° pulses were replaced by adiabatic Chirp pulses of 80 kHz width. Five coupling evolution delays (Δ) between 0.33 and 0.83 s were used and the scaling factor (κ) was set to $\kappa = \Delta/t_1$,max. The spectral width was 65 and 3 ppm in the indirect and direct dimensions, respectively. The experiments employing 16 transients were averaged for each of the 256 increments. Linear prediction to 512 points, zero-filling to about 8000 points and multiplication with a 90° shifted sine-bell function were performed prior to Fourier transformation in the indirect dimension. Coupling constants were subsequently determined from the peak separation in absolute value mode projections of the indirect dimension.

Raman and Raman optical activity measurements

The ROA spectra were measured at ambient temperature in water using the previously described ChiralRAMAN instrument (BioTools, Inc.),[27-28] which employs the scattered circular polarization (SCP) measurement strategy. The ROA spectra are presented as circular intensity differences (I_R-I_L) and the parent Raman spectra as circular intensity sums (I_R+I_L), with I_R and I_L denoting the Raman intensities with right- and left-circular polarization, respectively. The sample concentrations were 150 mM for all three disaccharides.

Experimental conditions: laser wavelength 532 nm; laser power at the sample 350 mW; spectral resolution 10 cm^{-1}; acquisition times ~17 h. Solvent water spectra were subtracted from the parent Raman spectra and all spectra were subsequently smoothed using a second level Savitzky-Golay filter.

Molecular Dynamics Simulations.

The glycosidic torsion angles were defined using H1'-C1'-On-Cn for ϕ and C1'-On-Cn-Hn (where n=2 or 3) for ψ in **M2M** and **M3M**. For **M6M**, the C1'-O6-C6-C5 torsion angle was used for ψ.

The MD simulations were performed using the CHARMM carbohydrate force field[54] together with the CHARMM,[55] and the modified TIP3P parameters for water.[56] The disaccharides were surrounded by water molecules in a cubic box with a side length equal to 29.972 Å. The particle-mesh Ewald method[57] was used for the long-range electrostatic interaction, and the remaining non-bonded interactions were shifted to zero between 10 and 12 Å. After energy minimization, the systems were heated from 100 to 298 K during 60 ps. Leap-frog integration was performed for 20 ns with a 2 fs time step and with constant pressure and temperature, keeping bonds to hydrogen atoms rigid using the SHAKE algorithm.[58,59]

Major conformational states were identified by inspecting the glycosidic torsion angle trajectories. Populations were determined by counting the fraction of the trajectories within limits defined by ψ > 10° and ψ < 10° for **M2M**, and ψ > 30° and ψ < 30° for **M3M**. For **M6M**, populations at the ω torsion angle were calculated using 120° ranges centered at 60°, −60°, and 180°, respectively for the gt, gg, and tg rotamers, while for ψ the states populations were defined as 0° – 120° for the clinal state and as 120° – 240° for the antiperiplanar conformation.

Representative coordinates from each conformational state in the simulations were obtained after recentering the trajectories around the sugar molecules.

Quantum mechanical calculations

Based on the population analysis, representative model structures of **M2M**, **M3M** and **M6M** were chosen for further refinement at DFT level. For the simplified approximations, e.g. gas phase and dielectric continuum (CPM) calculations, each structure was reoptimised at B3LYP/6-31G* level, with force field and ROA property tensors subsequently calculated at B3LYP/rDPS[60] level, either with or without a CPM background.

For the QM/MM level calculations, the two-layer ONIOM method, as implemented in GAUSSIAN09,[61] was chosen with the electronic embedding scheme, which incorporates the MM partial charges in the QM Hamiltonian. The initial geometries (with water boxes truncated to around 150 molecules) were again selected based on the MD population analysis, with the disaccharides making up the high/QM layer, computed at B3LYP/6-31G* level of theory.

The explicit water molecules represented the low/MM layer, computed with the AMBER (parm96) force field using TIP3P parameters. Two optimization methods were employed for the QM/MM calculations: full QM/MM and restricted QM/MM. The former allows full relaxation of all atoms in the system during the optimization, whilst the latter freezes the explicit water molecules so they retain the MD geometry and only the disaccharide is optimized. Full QM/MM calculations are computationally expensive because systems of this size, with explicit solvent molecules, have relatively flat potential energy surfaces and as such the convergence to the optimized geometry is slow. Restricted QM/MM is much less computationally intensive but offers poorer spectral prediction when comparing simulations to experiment.[20,21] The optimized snapshots were used as starting points for the frequency-dependent ROA tensor calculations. The fully analytical two-step procedure was used,[62] with force field calculations at the B3LYP/6-31G* level of theory and the ROA tensors calculated at the B3LYP/rDPS[60] level of theory, as recommended by Cheeseman and Frisch.[63]

In order to explicitly include water molecules at QM level, the normal mode partial optimization scheme was employed.[63] As input models, the same structures were used as in the QM/MM calculations, but the surrounding water box was further truncated to only include water molecules that directly hydrogen bonded to the disaccharide or in a hydrogen bonding network over the surface of the disaccharide, leaving ~15 water molecules per structure. These structures were partially optimized in GAUSSIAN09, interfacing with the QGRAD script,[64] at B3LYP/6-31G** level, allowing for a soft optimization without tearing away the water molecules. In order to mimic bulk water outside the hydrogen bonding range, a CPM background was added. After optimization, the two-step procedure was again employed to calculate the force field and ROA tensors, at B3LYP/6-31G** and B3LYP/rDPS level, respectively. A CPM continuum was added to all calculations.

For all predicted Raman and ROA output, the simulated incident laser wavelength for all ROA tensor calculations was set at the experimental value of 532 nm. Far from resonance, ROA intensities in the scattered circular polarization backscattered configuration (SCP-180) were obtained from the combination of appropriate invariants. Boltzmann and v4 factors were included to allow comparison against experimental spectra. All spectra were generated using a Lorentzian bandshape with a peak half-width of 10 cm-1. As absolute ROA intensities were not measured experimentally the calculated ROA intensities are compared in arbitrary units.

Overlap integral analysis

The similarities of the experimental Raman and ROA spectra with the corresponding theoretical spectra are calculated using the following formula that compares a computed spectrum ***f*** to an experimental spectrum ***g*** for a specific wavenumber range.

$$S_{fg} = \frac{\int_{300}^{1600} f(\sigma\tilde{\nu})g(\tilde{\nu})d\tilde{\nu}}{\sqrt{\int_{300}^{1600} f(\sigma\tilde{\nu})^2 d\tilde{\nu} \int_{300}^{1600} g(\tilde{\nu})^2 d\tilde{\nu}}}$$

The calculated spectrum has to be scaled in the wavenumber dimension with a scaling factor σ due to i.a. the harmonic approximation. The scaling factor σ is optimized varying from 0.950 to 1.000 in steps of 0.001 for the full spectral region. This generalised cosine measure S_{fg} is very popular in chiroptical spectroscopy since the numerator normalises its value and gives a similarity indication ranging from 0% to 100% for Raman spectra and from 100% to 100% for ROA spectra.[30,43-44] A negative S_{fg} can occur for differential spectra and indicates that the mirror image calculated spectrum is more similar to experimental spectrum.

The total similarity can be subdivided in different terms for different spectral regions as follows:

$$S_{fg} = \frac{\int_{300}^{950} f(\sigma\tilde{\nu})g(\tilde{\nu})d\tilde{\nu} + \ldots + \int_{1200}^{1600} f(\sigma\tilde{\nu})g(\tilde{\nu})d\tilde{\nu}}{\sqrt{\int_{300}^{1600} f(\sigma\tilde{\nu})^2 d\tilde{\nu} \int_{300}^{1600} g(\tilde{\nu})^2 d\tilde{\nu}}}$$

In this fashion, the contribution of each spectral region to the similarity of the entire spectrum can be assessed.

Acknowledgements

This work was supported by grants from the Swedish Research Council (no. 2013-4859 and 2017-03703) and the Knut and Alice Wallenberg Foundation. Computing resources were kindly provided by the Center for Parallel Computers (PDC), Stockholm, Sweden. P.L.A.P. acknowledges the EPSRC for funding through the award of an Established Career Fellowship (grant EP/K005472). Financial support by the BOF concerted research action '4D Protein Structure' is acknowledged.

Keywords: Carbohydrates •Density Functional Theory • Raman optical activity • Structure • Molecular Dynamics

[1] A. Varki, *Glycobiology* **2017**, *27*, 3.
[2] A. Imberty and S. Perez, *Chem. Rev.* **2000**, *100*, 4567.
[3] G. Widmalm, *Carbohydr. Res.* **2013**, *378*, 123.
[4] K. Gessler, I. Uson, T. Takaha, N. Krauss, S.M. Smith, S. Okada, G.M. Sheldrick and W. Saenger, *Proc. Natl. Acad. Sci. USA* **1999**, *96*, 4246.
[5] M. Färnbäck, L. Eriksson, S. Senchenkova, K. Zych, Y.A. Knirel, Z. Sidorczyk and G. Widmalm, *Angew. Chem. Int. Ed.* **2003**, *42*, 2543.
[6] K. Lycknert and G. Widmalm, *Biomacromolecules* **2004**, *5*, 1015.
[7] M. Yang, T.Angles d'Ortoli, E. Säwén, M. Jana, G. Widmalm and A.D. MacKerell Jr., *Phys. Chem. Chem. Phys.* **2016**, *18*, 18776.
[8] W. Zhang, T. Turney, R. Meredith, Q. Pan, L. Sernau, X. Wang, X. Hu, R.J. Woods, I. Carmichael and A.S. Serianni, *J. Phys. Chem. B* **2017**, *121*, 3042.
[9] H-C. Siebert, S. André, S-Y. Lu, M. Frank, H. Kaltner, J.A. van Kuik, E.Y. Korchagina, N. Bovin, E. Tajkhorshid, R. Kaptein, J.F.G. Vliegenhart, C-W. Von der Lieth, J. Jiménez-Barbero, J. Kopitz and H-J. Gabius, *Biochemistry* **2003**, *42*, 14762.
[10] C. Hamark, R. P-A. Berntsson, G. Masuyer, L.M. Henriksson, R. Gustafsson, P. Stenmark and G. Widmalm, *J. Am. Chem. Soc.* **2017**, *139*, 218.
[11] Z. Q. Wen, L. D. Barron and L. Hecht, *J. Am. Chem. Soc*., **1993** *115***,** 285.

[12] A. F. Bell, L. Hecht and L. D.Barron, *J. Am. Chem. Soc*., **1994** *116*, 5155.
[13] A. F. Bell, L. Hecht and L. D. Barron, *J. Raman Spectrosc*. **1995**, *26*, 1071.
[14] A. F. Bell, L. D. Barron and L. Hecht, *Carbohydr. Res*. **1994**, *257*, 11.
[15] A. F. Bell, L. Hecht, and L. D. Barron, *Spectrochim. Acta A* **1995**, *51*, 1367.
[16] F. Zhu, N.W. Isaacs, L. Hecht, G.E. Tranter and L.D. Barron, *Chirality* **2006**, *18*, 103.
[17] N.A. Macleod, C. Johannessen, L. Hecht, L.D. Barron and J.P. Simons, *Int. J. Mass Spectrom.* **2006**, *253*, 193.
[18] N.R. Yaffe, A. Almond and E.W. Blanch, *J. Am. Chem. Soc.* **2010**, *132*, 10654.
[19] J.R. Cheeseman, M.S. Shaik, P.L.A. Popelier and E.W. Blanch, *J. Am. Chem. Soc.* **2011**, *133*, 4991.
[20] S.T. Mutter, F. Zielinski, J.R. Cheeseman, C. Johannessen, P.L.A. Popelier and E.W. Blanch, *Phys. Chem. Chem. Phys.* **2015**, *17*, 6016.
[21] F. Zielinski, S.T. Mutter, C. Johannessen, E.W. Blanch and P.L.A. Popelier, *Phys. Chem. Chem. Phys.* **2015**, *17*, 21799.
[22] S.T. Mutter, F. Zielinski, C. Johannessen, P.L.A. Popelier and E.W. Blanch, *J. Phys. Chem. A* **2016**, *120*, 1908.
[23] L. D. Barron, *Molecular Light Scattering and Optical Activity*, 2nd ed, Cambridge University Press, Cambridge, **2004**.
[24] L. A. Nafie, *Vibrational Optical Activity*, Wiley, Chichester, **2011**.
[25] P. L. Polavarapu, *Chiroptical Spectroscopy*, CRC Press, Boca Raton, **2017**.
[26] L. D. Barron, L. Hecht, E. W. Blanch and A. F. Bell, *Prog. Biophys. Molec. Biol.* **2000**, *73*, 1.
[27] L. D. Barron, *Biomed. Spectrosc. Imaging* **2015**, *4*, 223.
[28] S. O. Pour, L. D. Barron, S. T. Mutter and E. W. Blanch, Raman optical activity, in *Chiral Analysis*, *Advances in Spectroscopy, Chromatography and Emerging Methods*, ed. P. L. Polavarapu, Elsevier, Amsterdam, **2018**, 249.
[29] V. Profant, A. Jegorov, P. Bouř and V. Baumruk, *J. Phys. Chem. B* **2017**, *121*, 1544.
[30] C. Mensch, L.D. Barron and C. Johannessen, *Phys. Chem. Chem. Phys.* **2016**, *18*, 31757.
[31] M. Górecki, *Org. Biomol. Chem.*, **2015** *13*, 2999.
[32] C. Johannessen and E. W. Blanch, *Curr. Phys. Chem.* **2013**, *3*, 140.
[33] P. Stanley, N. Taniguchi, M. Aebi, in *Essentials of Glycobiology*, ed. A. Varki, R.D. Cummings, J.D. Esko, P. Stanley, G.W. Hart, M. Aebi, A.G. Darvill, T. Kinoshita, N.H. Packer, J.H. Prestegard, R.L. Schnaar, P.H. Seeberger, Cold Spring Harbor Laboratory Press, Cold Spring Harbor (NY), 3rd Ed, **2015-2017**, chapter 9, p. 99.
[34] S.W. Homans, A. Pastore, R.A. Dwek and T.W. Rademacher, *Biochemistry* **1987**, *26*, 6649.
[35] T. Srikrishnan, M.S. Chowdhary and K.L. Matta, *Carbohydr. Res.* **1989**, *186*, 167.
[36] R.J. Woods, C.J. Edge and R.A. Dwek, *Nat. Struc. Biol.* **1994**, *1*, 499.
[37] E.W. Sayers and J.H. Prestegard, *Biophys. J.* **2000**, *79*, 3313.
[38] S. Jo, Y. Qi and W. Im, *Glycobiology* **2016**, *26*, 19.
[39] C. Johannessen, R. Pendrill, G. Widmalm, L. Hecht and L.D. Barron, *Angew. Chem. Int. Ed.* **2011**, *50*, 5349.
[40] E. Säwén, T. Massad, C. Landersjö, P. Damberg and G. Widmalm, *Biomol. Chem.* **2010**, *8*, 3684.
[41] D.S. Patel, R. Pendrill, S.S. Mallajosyula, G. Widmalm and A.D. MacKerell Jr., *J. Phys. Chem. B*, **2014** *118*, 2851.
[42] U. Olsson, E. Säwén, R. Stenutz and G. Widmalm, *Chem. Eur. J.* **2009**, *15*, 8886.
[43] T. Kuppens, W. Langenaeker, J. P. Tollenaere and P. Bultinck, *J. Phys. Chem. A* **2003**, *107*, 542.
[44] C. L. Covington and P. L. Polavarapu, *J. Phys. Chem. A* **2013**, *117*, 3377.
[45] T. Kuppens, K. Vandyck, J. Van der Eycken, W. Herrebout, B. J. van der Veken and P. Bultinck, *J. Org. Chem.* **2005**, *70*, 9103.
[46] T. Kuppens, K. Vandyck, J. van der Eycken, W. Herrebout, B. van der Veken and P. Bultinck, *Spectrochim. Acta - Part A Mol. Biomol. Spectrosc.* **2007**, *67*, 402.
[47] E. Debie, E. De Gussem, R. K. Dukor, W. Herrebout, L. A. Nafie and P. Bultinck, *ChemPhysChem* **2011**, *12*, 1542.
[48] C. Mensch and C. Johannessen, *ChemPhysChem* **2018**, DOI: 10.1002/cphc.201800924
[49] S.Y. Liem and P.L.A. Popelier, *Phys. Chem. Chem. Phys.* **2014**, *16*, 4122.
[50] K.J. Naidoo and JY-J. Chen, *Mol. Phys.* **2003**, *101*, 2687.
[51] D.Wang, M.L. Amundadottir, W.F. van Gunsteren and P.H. Hunenburger, *Eur. Biophys. J.* **2013**, *42*, 521.
[52] A. Rüther, A. Forget, A. Roy, C. Carballo, F. Mießmer, R.K. Dukor, L.A. Nafie, C. Johannessen, V.P. Shastri and S. Lüdeke, *Angew. Chem. Int. Ed.* **2017**, *129*, 4674.
[53] A. Meissner and O. W. Sørensen, *Magn. Reson. Chem.* **2001**, *39*, 49.
[54] O. Guvench, E. Hatcher, R.M. Venable, R.W. Pastor and A.D. MacKerell Jr., *J. Chem. Theory Comput.* **2009**, *5*, 2353.
[55] B. R. Brooks, C.L. Brooks III, A.D. Mackerell Jr., L. Nilsson, R.J. Petrella, B. Roux, Y. Won, G. Archontis, C. Bartels, S. Boresch, A. Caflisch, L. Caves, Q. Cui, A.R. Dinner, M. Feig, S. Fischer, J. Gao, M. Hodoscek, W. Im, K. Kuczera, T. Lazaridis, J. Ma, V. Ovchinnikov, E. Paci, R.W. Pastor, C.B. Post, J.Z. Pu, M. Schaeffer, B. Tidor, R.M. Venable, H.L. Woodcock, X. Wu, W. Yang, D.M. York and M. Karplus, *J. Comput. Chem.* **2009**, *30*, 1545.
[56] W.L. Jorgensen, J. Chandrasekhar and J.D. Madura, *J. Chem. Phys.* **1983**, *79*, 926.
[57] S.E. Feller, R.W. Pastor, A. Rojnuckarin, S. Bogusz and B.R. Brooks, *J. Phys. Chem.* **1996**, *100*, 17011.
[58] J-P. Ryckaert, G. Ciccotti and H.J.C. Berendsen, *J. Comput. Phys*. **1977**, *23*, 327.
[59] W.F. van Gunsteren and H.J.C. Berendsen, *Mol. Phys.* **1977**, *34*, 1311.
[60] G. Zuber and W. Hug, *J. Phys. Chem. A* **2004**, *108*, 2108.
[61] M. J. Frisch, G. W. Trucks, H. B. Schlegel, G. E. Scuseria, M. A. Robb, J. R. Cheeseman, G. Scalmani, V. Barone, B. Mennucci, G. A. Petersson, H. Nakatsuji, M. Caricato, X. Li, H. P. Hratchian, A. F. Izmaylov, J. Bloino, G. Zheng, J. L. Sonnenberg, M. Hada, M. Ehara, K. Toyota, R. Fukuda, J. Hasegawa, M. Ishida, T. Nakajima, Y. Honda, O. Kitao, H. Nakai, T. Vreven, J. A. Montgomery Jr, J. E. Peralta, F. Ogliaro,M. J. Bearpark, J. Heyd, E. N. Brothers, K. N. Kudin, V. N. Staroverov, R. Kobayashi, J. Normand, K. Raghavachari, A. P. Rendell, J. C. Burant, S. S. Iyengar, J. Tomasi, M. Cossi, N.Rega, N. J.Millam,M.Klene, J.E.Knox, J.B. Cross,V.Bakken, C. Adamo, J. Jaramillo, R. Gomperts, R. E. Stratmann, O. Yazyev, A. J. Austin, R. Cammi, C. Pomelli, J. W. Ochterski, R. L.Martin, K. Morokuma, V. G. Zakrzewski, G. A. Voth, P. Salvador, J. J. Dannenberg, S. Dapprich, A. D. Daniels, O. Farkas, J. B. Foresman, J. V. Ortiz, J. Cioslowski and D. J. Fox, Gaussian, Inc., Wallingford, CT, USA, **2009**.
[62] K. Ruud and A.J. Thorvaldsen, *Chirality* **2009**, *21*, E54.
[63] J.R. Cheeseman and M.J. Frisch, *J. Chem. Theory Comput.* **2011**, *7*, 3323.
[64] P. Bouř and T.A. Keiderling, *J. Chem. Phys.* **2002**, *117*, 4126